A transfer matrix for the backbone exponent of two-dimensional percolation

2002 J. Phys. A: Math. Gen. 35 2131

(http://iopscience.iop.org/0305-4470/35/9/304)

INSTITUTE OF PHYSICS PUBLISHING JOURNAL OF PHYSICS A: MATHEMATICAL AND GENERAL

J. Phys. A: Math. Gen. **35** (2002) 2131–2144 PII: S0305-4470(02)31244-7

A transfer matrix for the backbone exponent of two-dimensional percolation

Jesper Lykke Jacobsen and Paul Zinn-Justin

Laboratoire de Physique Théorique et Modèles Statistiques, Université Paris-Sud, Bâtiment 100, 91405 Orsay Cedex, France

Received 22 November 2001
Published 22 February 2002
Online at stacks.iop.org/JPhysA/35/2131

Abstract

Rephrasing the backbone of two-dimensional percolation as a monochromatic path crossing problem, we investigate the latter by a transfer matrix approach. Conformal invariance links the backbone dimension D_{b} to the highest eigenvalue of the transfer matrix $\mathbf{T}$, and we obtain the result $D_{\mathrm{b}} = 1.6431 \pm 0.0006$. For a strip of width L, $\mathbf{T}$ is roughly of size 2^{3^L}, but we manage to reduce it to $\sim L!$. We find that the value of D_{b} is stable with respect to inclusion of additional 'blobs' tangent to the backbone in a finite number of points.

PACS numbers: 64.60.Ak, 02.10.Yn, 05.50.+q, 11.25.Hf

1. Introduction

The critical behaviour of percolation has attracted considerable interest in the mathematical physics literature over the last decades. Whereas most practical applications (such as studying the efficiency of oil extraction from a porous soil, or the fractal geometry of a strike of lightning) take place in three spatial dimensions, analytical progress has largely been confined to two dimensions [1]. Although of geometric origin, percolation fits in the framework of critical phenomena, and in particular the concept of universality should apply. One therefore expects the specific choice of a discrete model (bond or site percolation) and the lattice structure (e.g. square or triangular) to be of no relevance to the determination of the critical exponents.

A large part of the progress made is due to the identification with the $q \to 1$ limit of the q-state Potts model [1]. A very fruitful idea has been to treat the latter in terms of its random cluster formulation [2], and further in terms of the loops surrounding the clusters [3]. Applying Coulomb gas (and related) methods to the loop model led to a range of exact results around 1980 [4]. In particular, the correlation length exponent $\nu = \frac{4}{3}$ [5] and the magnetic exponent $x_h = \frac{5}{48}$ [6, 7] (the codimension of which is the fractal dimension of the percolating cluster, $D = 2 - x_h = \frac{91}{48}$) were computed.

The next major advance followed from the advent of conformal field theory [8], which provides an appealing correspondence between the q-state Potts model (for particular values of q) and the so-called minimal models. For instance, the exponents $x_k = \frac{1}{12}(k^2 - 1)$, with $k \geqslant 2$ [9, 10], describing the asymptotic decay of the probability $P_k(r) \sim r^{-2x_k}$ of having k loop segments connecting two narrow regions over a distance $r \gg 1$ [4], were found to fit in the Kac table of conformal dimensions [11]. Another remarkable result is the celebrated Cardy formula [12] expressing certain path-crossing probabilities in terms of hypergeometric functions.

More recently, percolation has attracted the interest of probabilists. In a ground-breaking paper, Smirnov has proved that the scaling limit of site percolation on the triangular lattice exists and is described by the stochastic Loewner evolution with parameter $\kappa = 6$ [13]. Consequently, most of the results referred to in the above have now been rigorously proved.

Nevertheless, a certain class of exponents have continued to resist the physicists' attempts over the years. These are most conveniently defined by considering bond percolation inside a large square, of which we imagine two opposing sides to be connected to superconducting plates (see figure 1). Each percolating bond is stipulated to possess a fixed and finite conductivity, and an electric voltage is applied across the plates. At the percolation threshold $p = p_c$, the part of the network that supports a non-zero current is known as the *backbone*, and its fractal dimension D_b determines a critical exponent $\tilde{x}_2 = 2 - D_b$. Near p_c, the conductivity of the network scales as $(p - p_c)^t$, defining the conductivity exponent t. The latter can be connected to the fractal dimension of random walks constrained to the percolating cluster, or to its backbone, via the Einstein relation [14].

A number of conjectures for $\tilde{x}_2$ have been falsified as numerical simulations have become increasingly accurate. The benchmark thus far is the Monte Carlo method of Grassberger [15] in which the conducting part of the cluster is identified using a clever recursive algorithm. Large-scale simulations yield the value $\tilde{x}_2 = 0.3568 \pm 0.0008$ [16]. The exponent $\tilde{x}_2$ is actually a member of a family of the so-called monochromatic path-crossing exponents $\tilde{x}_k$ [10], with the magnetic exponent fitting in as $x_h = \tilde{x}_1$. The higher exponents $\tilde{x}_k$, $k \geqslant 3$, are all unknown.

In the present paper we provide a numerical estimate of $\tilde{x}_2$ using an algorithm which is entirely different from that of Grassberger. Using the reformulation of $\tilde{x}_2$ as a path-crossing problem, we relate it to the largest eigenvalue of a linear operator (actually a transfer matrix) that builds all possible percolation clusters supporting at least $k = 2$ mutually non-intersecting paths. We work in the geometry of semi-infinite strips of width L, with $L \leqslant 9$.

Our approach is interesting in several respects. First, the reformulation as an eigenvalue problem makes direct contact with the predictions of conformal field theory [17]. That Grassberger's recursive algorithm defines a conformally invariant observable is not *a priori* obvious, but the fact that the transformation to a path-crossing problem involves a conformal transformation and that here we obtain a consistent value of $\tilde{x}_2$ shows that this is indeed the case. One would then further expect $\tilde{x}_2$ to be the conformal dimension of a primary operator $\hat{O}_2$ in some (presently unknown) conformal field theory of percolation. In particular, the conformal tower of $\hat{O}_2$ should possess descendents whose conformal dimensions are integer-spaced with respect to $\tilde{x}_2$. We have checked this prediction by examining the scaling of the first few eigenvalues of our transfer matrix with system size. We shall present evidence of a level two descendent with conformal dimension 2.35 ± 0.1, whereas there does not appear to be a descendent at level one.

Second, the generalization of our method to the case of more ($k \geqslant 3$) paths, or to the Potts model with $q \neq 1$ states, is immediate. Results for these cases will appear in a separate paper [18]. Third, from a technical point of view we have had to tackle the major obstacle of writing a transfer matrix in which some degrees of freedom (the percolation clusters) must be summed over, whereas others (the paths) act as constraints on the former but must not themselves be summed over. Fourth, we have devised an algorithm which is naturally parallelizable.

Similar to Grassberger [16] we find that the data for $\tilde{x}_2$ are hampered by strong (presumably non-analytical) corrections to scaling. As a consequence our final result

$$\tilde{x}_2 = 0.3569 \pm 0.0006 \tag{1.1}$$

confirms that of [16], but unfortunately does not improve its precision. On the other hand, we have devised some variants of our algorithm in which the constraint of mutual avoidance of the two paths is relaxed, so that they are allowed to touch in some configurations at vertices but not to share an edge. Physically this means that we measure the fractal dimension of the backbone with some 'blobs' that are tangent to it included. The surprising result is that this relaxation of the original definition does not alter the value of $\tilde{x}_2$.

The paper is laid out as follows. In section 2 we review the reasoning leading from the original formulation of the backbone dimension to that of a path-crossing problem, and restate the latter in a strip geometry. The construction of the corresponding transfer matrix, and of its associated state space, is described in section 3. In section 4 we transcribe this as an algorithm and discuss its implementation. The data are analysed and extrapolated to the $L \to \infty$ limit in section 5. The appendix displays some transfer matrices produced for small system size.

Note added: When this work was being completed we became aware of the preprint of Lawler *et al* [19] in which $\tilde{x}_1 = \frac{5}{48}$ is established on a rigorous basis, following Smirnov [13]. The authors also relate $\tilde{x}_2$ to a second-order partial differential equation with specific boundary conditions, but fail to provide an explicit solution of the latter. We thank John Cardy for bringing this to our attention.

2. Path-crossing probabilities

Let us return to the formulation of the backbone problem given in the introduction, namely in the so-called busbar geometry (see figure 1). The condition that a given point (site or bond, as

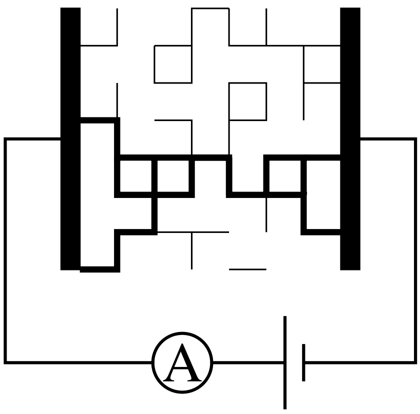

Figure 1. Busbar geometry, here shown for the case of bond percolation on the square lattice. The backbone is indicated by thick edges.

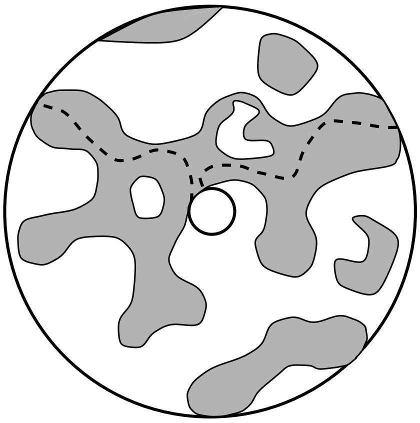

Figure 2. Annular geometry endowed with critical percolation (here shown in the continuum limit). A possible choice of two disjoint percolating paths is shown as dashed lines.

the case may be) on the spanning cluster belongs to the backbone is that it can be connected to either of the superconducting plates by means of two mutually non-intersecting paths[1].

This choice of geometry is somewhat unnatural, as it does not fully display the rotational symmetry of the continuum limit. It is more convenient to work in an annular geometry limited by two concentric circles of radii $r \ll 1$ and $R \gg 1$. Interpreting the inner circle as the point which is a potential element of the backbone and the outer as the point at infinity, we see that a given percolating configuration in the annulus contributes to the backbone if and only if the two circles are connected by two mutually non-intersecting paths on the percolating cluster(s) (see figure 2).

More generally, one may define higher exponents $\tilde{x}_k$ by studying, at the percolation threshold, the probability $P_k(r, R) \sim \left(\frac{r}{R}\right)^{\tilde{x}_k}$ that the annulus is traversed by k mutually non-intersecting paths. Clearly, the configurations in which these paths belong to different clusters are asymptotically subdominant, and so we might as well assume that they belong to the same cluster.

The situation may be further refined [10] by considering path-crossing events in which a given number of traversing paths belong to the clusters, and the remainder belong to the dual clusters[2]. More precisely, for each k there are 2^k types of path configurations, each specified by a set of colour variables $(\tau_1, \tau_2, \ldots, \tau_k)$ with $\tau_i = +1$ (respectively $\tau_i = -1$), which means that path number i belongs to the clusters (respectively, to the dual clusters). Within the context of the q-state Potts model (with $q \neq 1$), it is not obvious whether different choices of the colour variables will lead to the same critical exponents, except of course for the obvious symmetries obtained by rotating the sequence $(\tau_1, \tau_2, \ldots, \tau_k)$, reversing its order, or dualizing it. But in the percolation case ($q = 1$) the bonds (or sites) are uncorrelated, and various parts of the system may be dualized independently. Using this approach, it has been proved in the case of site percolation on the triangular lattice [10] that all the polychromatic sequences (in which both $\tau_i = +1$ and $\tau_j = -1$ are represented; $k \geqslant 2$) share the same critical exponents. In particular, any polychromatic colour configuration may be transformed into the alternate one, $\tau_i = (-1)^i$.

[1] Strictly speaking, this condition also includes points which are being held exactly at zero current in a Wheatstone bridge-like arrangement. Since in the continuum limit the percolation cluster is almost surely ‘asymmetric’, such points are extremely rare. Also see the discussion below on the possibility of contact points for paths.

[2] For site percolation, the dual clusters consist of the non-conducting (uncoloured, white) sites. For bond percolation on the square lattice, it is most natural to think of the dual clusters in terms of the standard duality transformation in the random cluster model [2], according to which any conducting edge is intersected by a non-conducting dual edge, and vice versa.

We expect this result to be independent of a particular lattice realization, and thus to apply also to the bond percolation. In this case, the identification of the critical exponent with that of k traversing loop segments on the surrounding lattice, referred to as x_k in the introduction, becomes evident (at least for k even). A rigorous proof that the formula $x_k = \frac{1}{12}(k^2 - 1)$ applies to the polychromatic path-crossing problem for site percolation on the triangular lattice was spelt out in [10].

For monochromatic sequences (all $\tau_i = +1$) the argument given in [10] fails, and the corresponding exponents $\tilde{x}_k$ are expected to be different from the x_k. Indeed, from entropic considerations it should be clear that $x_k < \tilde{x}_k < x_{2k}$.

Several of the x_k have nice physical interpretations. Thus, x_2, x_3 and x_4 are, respectively, the codimensions of the cluster perimeter (hull) [9], the external (accessible) perimeter [10] and the set of pivotal (singly connecting) bonds [9]. The latter also yields the correlation length exponent [5], via the scaling relation $\nu = 1/(2 - x_4)$.

In the absence of an exact solution, one might imagine evaluating the exponents $\tilde{x}_k$ numerically by measuring the decay of the path-crossing probabilities on an annulus, as outlined above. A more feasible alternative is to compute certain restricted free energies on semi-infinite cylinders by using a transfer matrix, as we shall describe in the next section. These free energies can be related to the critical exponents as follows.

Since the scaling limit of critical percolation is conformally invariant [8, 13], one is allowed to transform the annular geometry of figure 2 into a cylindrical one by means of the conformal mapping $w \equiv u + \mathrm{i}v = \frac{L}{2\pi}\log(z)$. The transformed complex coordinate w may be thought of as embedded in the strip $-\infty < u < \infty$, $0 \leqslant v \leqslant L$ with periodic boundary conditions in the v-direction. This means that figure 2 must be viewed in perspective, interpreting the inner and outer circles as the extremities of the cylinder.

We are going to make use of the following result: let $f_0(L)$ be the free energy per unit area for the unrestricted percolation problem, and $\tilde{f}_k(L)$ (respectively $f_k(L)$) the corresponding quantity for the constrained problem where only those configurations are included in the partition sum in which (at least) k monochromatic (respectively polychromatic) paths span the length of a semi-infinite cylinder of width L. Then as $L \to \infty$, the discrete lattice model, at criticality, should have a continuum limit described by the conformal field theory, so that [17]

$$\tilde{f}_k(L) - f_0(L) = \frac{2\pi\tilde{x}_k}{L^2} + o(L^{-2}) \tag{2.1a}$$

$$f_k(L) - f_0(L) = \frac{2\pi x_k}{L^2} + o(L^{-2}). \tag{2.1b}$$

We shall obtain estimates for the $\tilde{x}_k$ by extrapolating data for sufficiently large strips to the limit $L \to \infty$.

3. Transfer matrix algorithm

It has been known for a long time how to numerically compute the $f_k(L)$, by writing the transfer matrix for the loop model [3] on the basis of planar (Catalan-like) connectivities (see [20] for a closely related computation). The same is true for $\tilde{f}_1(L)$ by using the trick of adding a ghost site [21], or alternatively (via a duality argument) by forbidding the clusters to wrap around the cylinder [22].

The computation of $\tilde{f}_2(L)$, the principle of which we now describe, is considerably more complicated. The main complication stems from the fact that to compute the corresponding partition sum we must exclude those configurations of the percolation clusters that do not support (at least) two spanning paths, and count each of those that do with *unit weight* (and not

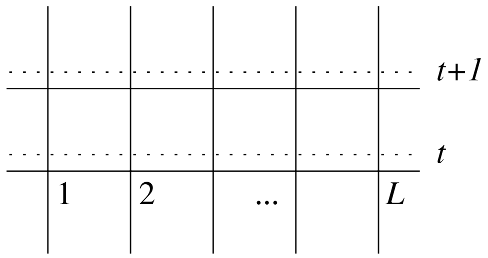

Figure 3. The square lattice with periodic boundary conditions along one of its orientations. The dotted lines are time slices.

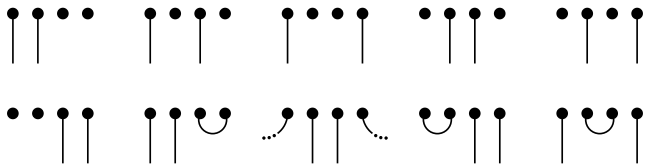

Figure 4. The ten possible path configurations for $L = 4$.

with a weight equal to the number of ways two such paths can be realized for the given cluster configuration). Roughly speaking, the degrees of freedom are the clusters *and* the paths, and we must trace over the former but *not* the latter.

For the sake of definiteness we consider in this section critical *bond* percolation on a square lattice, though the principle of the transfer matrix can be applied to any lattice with any probability of occupation p, and to bond as well as site percolation. Since in our case $p_c = \frac{1}{2}$ [1], it is convenient to simply assign a weight of one to every configuration of percolating/non-percolating bonds. For now we consider the simplest orientation of the lattice, which corresponds to L sites in the transverse direction with periodic boundary conditions (figure 3). With all these conventions, $f_0(L) = -2\log 2$ in equation (2.1a). We shall discuss later another possible orientation of the lattice.

We keep track of the paths by defining path configurations in analogy with those used in the transfer matrix calculations of the self-avoiding walk [23]: among the L sites in a row (at time $t = t_0$), two sites are connected to the point at infinity (time $t = -\infty$) by means of paths. Furthermore, in order to allow subsequent backtracking of either path (at a later instant $t > t_0$), the remaining sites may be connected in pairs by means of backward arches. The possible configurations for $L = 4$ are listed in figure 4.

To overcome the difficulty of not summing over the possible path configurations, we define the basis states on which the transfer matrix acts as *lists* of path configurations. Elements of the list give all possible realizations of the positions of the paths (and of the arches) which are compatible with the 'past' of the state.

Formally, if $\mathcal{P}$ is the set of path configurations, then basis states are indexed by non-empty subsets of $\mathcal{P}$ (one must exclude the empty subset since it corresponds to states for which there is no possibility of two disjoint paths reaching time t). Note that the dimension of the total space is $2^{\#\mathcal{P}} - 1$, which grows extremely rapidly with L. We shall return to this point when we discuss practical implementation.

By definition, the matrix element $\mathbf{T}_{\mathcal{A}\mathcal{B}}$ between basis states indexed by $\mathcal{A} \subset \mathcal{P}$ and $\mathcal{B} \subset \mathcal{P}$ equals the number of configurations of the bonds between time t and time $t + 1$, such that the state $\mathcal{A}$ at time $t + 1$ is obtained from the state $\mathcal{B}$ at time t. Given the initial state $\mathcal{B}$ and the

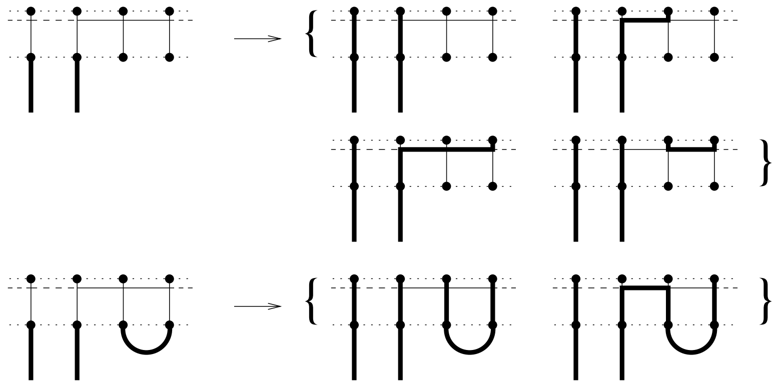

Figure 5. Evolution of two path configurations with the same percolation configuration. Solid (respectively dashed) lines represent percolating (respectively non-percolating) bonds, whereas thick lines represent the possible paths.

configuration of the bonds $\omega \in \Omega$ (that is whether they are percolating or not, Ω being the set of all possibilities), the procedure to determine the final state $\mathcal{A}$ is as follows:

- For each possible initial path configuration $b \in \mathcal{B}$, consider all possible continuations of the existing lines at time t (the two original paths and the arches) that are compatible with the configuration of the bonds ω. Note that each line must be either continued to a site at time $t + 1$ or connected to another line (in which case it will re-emerge at the other end of the arch; the lines coming from infinity or from the same arch cannot be connected to each other). Furthermore, for each pair of adjacent empty sites, one must consider the possibility of creating a new arch. Let $\phi(b, \omega) \subset \mathcal{P}$ be the list of path configurations at $t + 1$ thus produced.
- The full state $\mathcal{A}$ is reconstructed by simply putting together all the possibilities (of the form $\phi(b, \omega)$, $b \in \mathcal{B}$) obtained for each initial path configuration. If one finds $\mathcal{A} = \emptyset$, this means that no continuation is possible, and the state is excluded.

We give an example of such a computation in figure 5.

In other words, we have the formal identity

$$\mathbf{T}|\mathcal{B}\rangle = \sum_{\omega\in\Omega} \Big|\bigcup_{b\in\mathcal{B}} \phi(b, \omega)\Big\rangle$$

which shows quite explicitly that one sums over bond configurations but not over path configurations.

Finally, the free energy per unit area is given by

$$\tilde{f}_2(L) = -\lim_{t\to\infty} \frac{1}{Lt} \log\langle\mathcal{A}|\mathbf{T}(L)^t|\mathcal{B}\rangle \tag{3.1}$$

where the states $\mathcal{A}$, $\mathcal{B}$ specify the boundary conditions and are essentially arbitrary (the state $\mathcal{A}$ should belong to the image of $\mathbf{T}$, see the next section), and $\mathbf{T}(L)$ is the transfer matrix for strip width L.

As $t \to \infty$, the matrix element $\langle\mathcal{A}|\mathbf{T}(L)^t|\mathcal{B}\rangle$ is dominated by the largest eigenvalue $\lambda(L)$ of $\mathbf{T}(L)$, and combining equations (2.1a) and (3.1), we find:

$$\frac{1}{2^{2L}}\lambda(L) = 1 - \frac{2\pi\tilde{x}_2}{L} + o(L^{-1}). \tag{3.2}$$

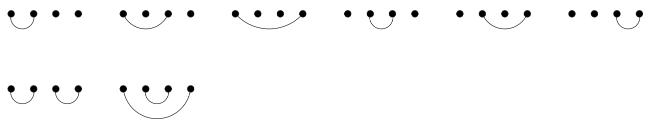

Figure 6. The configurations of figure 4 redrawn as arches.

4. Algorithmic details

In order to appreciate how effective the transfer matrix approach is, it is important to understand the structure of the matrix constructed in the previous section. It is an integer-valued matrix of extremely large size, but many of its entries are zero. In fact, starting from any basis state $|\mathcal{B}\rangle$, a very limited number of states are generated. These are the only states that matter for the determination of the largest eigenvalue(s) and we can thus restrict ourselves to a submatrix of much smaller size.

We now describe schematically the procedure we used. The main steps of the algorithm are as follows:

(i) Start with an arbitrary basis state (ideally, one that we know is generated by iteration of the transfer matrix). Put it onto a 'stack' of states for processing.

(ii) Pick a state $\mathcal{B}$ from the stack and 'process' it, i.e. generate the non-zero entries $\mathbf{T}_{\mathcal{AB}}$, and store them. This encodes one column of the transfer matrix.

(iii) Consider every new basis state $\mathcal{A}$ that has been generated at step (ii); check if it has already been processed; if not, add it to the stack. If the stack is non-empty, go back to step (ii).

(iv) Finally, once the stack is empty, the largest eigenvalue is computed by simple iteration of the matrix that has been generated.

The transfer matrix is such that the submatrix thus generated has no zero rows or columns. We call this submatrix the reduced transfer matrix.

An important remark for practical applications is that this procedure is highly parallelizable: several CPUs can perform step (ii) simultaneously and independently; only the stack must be shared. In practice, it is necessary to have a server that communicates with various clients involved in the computation; it ensures that their stacks are synchronized, and dispatches the tasks. At the end of each calculation (step (ii)), a client sends the server the new states created and receives the states created by other clients in the meantime. The time spent updating the stack being very small compared to the calculation time, the parallelization is near 100% efficient (at least up to 20 clients which is the maximum we tested).

Let us now discuss this procedure in more detail.

First, we must define how to encode path configurations. A study of figure 4 shows that if exactly $k = 2$ paths are connected to $t = -\infty$, then they can be considered as an extra arch. This trick reduces the number of configurations and slightly simplifies the implementation (but cannot be extended to $k \neq 2$). We can then move the point at infinity and redraw the configurations as standard arch configurations[3] (see figure 6).

An arch configuration is then encoded in a standard way as a sequence of closing/empty/opening steps, i.e $\epsilon_i \in \{-1, 0, +1\}$, $1 \leqslant i \leqslant L$, such that the height function

[3] The number of L-point arch configurations equals $m_L - 1$, where m_L are the Motzkin numbers [24] (the empty configuration is excluded). The generating function $M(x) \equiv \sum_{L=0}^{\infty} m_L x^L = (1 - x - \sqrt{1 - 2x - 3x^2})/2x^2$ has a singularity in $x = x_c = \frac{1}{3}$, showing that the number of path configurations is $m_L \approx 3^L$ asymptotically.

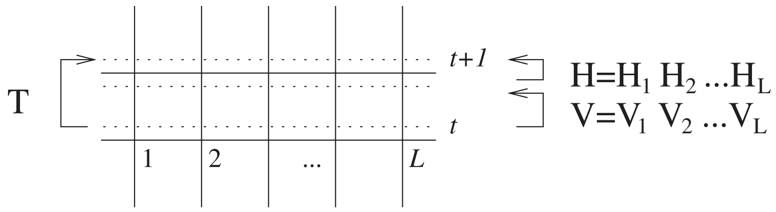

Figure 7. Factorization of the transfer matrix.

$h_\ell = \sum_{i=1}^{\ell} \epsilon_i$ satisfies $h_\ell \geqslant 0$ for all ℓ and $h_L = 0$. States are now defined as sorted lists of path configurations.

Next, we discuss how to perform step (ii) in practice. One possibility would be to directly apply the principle of section 3, that is to consider all possible bond configurations between two successive time slices, and for each, to produce the resulting state. However, since there are 2^{2L} such configurations, the time required to do so grows exponentially, which is not satisfactory. Besides, the determination of all possible continuations of the paths to time $t+1$ is a rather complex task. Instead, we shall use a factorization of the transfer matrix as a product of L sparse matrices $\mathbf{T}_i$, $1 \leqslant i \leqslant L$, which describe the addition of a single site. The details of the factorization depend on the exact situation envisioned. We present here three cases.

4.1. The square lattice with standard orientation

The example used so far is that of the square lattice with its usual orientation. In this case the factorization can be pushed further by writing $\mathbf{T}(L) = \mathbf{H}_1 \cdots \mathbf{H}_L \mathbf{V}_1 \cdots \mathbf{V}_L$, where $\mathbf{V}_i$ (respectively $\mathbf{H}_i$) corresponds to the addition of a single vertical (respectively horizontal) bond (figure 7).

The action of $\mathbf{V}_i$ is very simple: $\mathbf{V}_i = \mathbf{V}'_i + \mathbf{V}''_i$, where $\mathbf{V}'_i$ (respectively $\mathbf{V}''_i$) describes the evolution when the vertical bond number i is percolating (respectively non-percolating). $\mathbf{V}'_i$ is simply the identity, whereas $\mathbf{V}''_i$ acts on path configurations as follows: either a path/arch is at site i, in which case it gives 0 (the path cannot cross the non-percolating bond), or there is not, which is the identity. The action on a state made of *several* path configurations can be deduced from these basic rules, as explained in section 3.

The action of $\mathbf{H}_i$ is slightly more complicated: $\mathbf{H}_i = \mathbf{H}'_i + \mathbf{H}''_i$, similarly as above. The definitions of $\mathbf{H}'_i$ and $\mathbf{H}''_i$ must take into account all the possibilites of continuations, recombinations and creations of paths along the horizontal bonds. This requires working, as intermediate states, with path configurations of length $L+2$ instead of L, since one must temporarily distinguish the paths directed horizontally and vertically at the first and last vertices being currently processed. We leave the details as an exercise to the interested reader.

A final ingredient is that one can use the dihedral symmetry of the transfer matrix: since the latter commutes with cyclic permutations of the sites and with reflections, one can select a representative in each orbit of the dihedral group among the basis states. Note that the action is an overall action on all configurations that constitute the state simultaneously. The states generated by the above procedure can then be replaced with the representative state of their orbit, producing a smaller transfer matrix but with identical eigenvalues. This further reduces the size of the transfer matrix by a factor of (roughly) L.

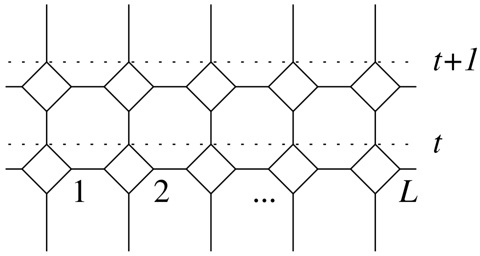

Figure 8. Deformation of the square lattice.

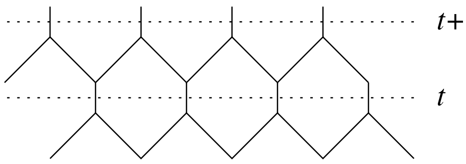

Figure 9. Another deformation of the square lattice.

4.2. The square lattice with standard orientation 2: the square/octagon deformation

It is interesting to study variants of the algorithm above. One natural question is: if one allows the paths to touch each other at *vertices*, how is the asymptotic behaviour of the free energy modified and in particular is $\tilde{x}_2$ left unchanged? Another possible formulation of this question is to consider a deformation of the lattice in which each vertex is replaced with a small square, resulting in a square/octagon lattice (figure 8). The bonds of the small square are always percolating and allow paths that would have touched at a vertex to avoid each other[4].

Physical insight suggests that such modifications should not affect the values of $\tilde{x}_2$. The reason is that, just like the Wheatstone bridge configurations mentioned in the introduction, the fact that current flows through loops which are connected to the backbone by just one point is rather unstable since any microscopic defect that breaks the symmetry between the two orientations of the loops (deforming the lattice is precisely a way of introducing such a defect) will produces a non-zero current. If $\tilde{x}_2$ is to be universal it should not depend on such microscopic details. It is this insight that we would like to test. There is another, more practical reason one would want to study such modifications of the algorithm, which will be apparent in section 5.

It is very simple to modify the transfer matrix of section 4.3 to allow such path evolutions. V_i is unchanged, whereas H_i now allows two paths to reach the same vertex and emerge from it as if they had not touched each other.

4.3. The square lattice with light-cone orientation: the hexagon deformation

Finally, we rotate the lattice by 45°, the motivation being that we expect better convergence properties, as observed empirically in similar computations [22, 25]. Unfortunately, there is no efficient way to encode the corresponding configurations, and we are therefore led to a modification of the lattice which is similar to what was done in section 4.2: this time the result is a hexagon lattice in which vertical bonds are always percolating (figure 9). This is equivalent to allowing 'horizontal tangencies' on the original square lattice, that is allowing two paths to touch at one vertex in the configuration where the two upper edges belong to the same path; however, 'vertical tangencies' are still excluded.

In this case, encoding the states becomes completely identical to what was done previously. There is a decomposition $\mathbf{T} = \mathbf{T}_1 \cdots \mathbf{T}_L$ where $\mathbf{T}_i$ adds an extra vertex i at time $t+1$ (and two bonds). Since the new sites at $t+1$ are now shifted with respect to the sites at t, the action of the transfer matrix includes a conventional rotation of a half-bond length (or π/L).

[4] Note that a path crossing a vertex of the original lattice can correspond to two different paths on the deformed lattice, but since we do not sum over path realizations this is of no consequence.

Table 1. Size of the reduced transfer matrix.

L	4	5	6	7	8	9
s_1	15	72	515	4219	41 728	?
s_2	12	51	291	1893	14 923	132 799
s_3	12	51	291	1893	14 923	132 799

Table 2. Largest eigenvalue of the transfer matrix. The last column shows the second real eigenvalue for the third transfer matrix.

L	$\lambda_1/2^{2L}$	$\lambda_2/2^{2L}$	$\lambda_3/2^{2L}$	$\lambda'_3/2^{2L}$
4	0.514 287 790 945	0.540 388 840 500	0.718 747 415 570	0.058 692 638 251
5	0.594 678 112 301	0.617 254 658 842	0.775 012 703 547	0.145 046 191 784
6	0.653 760 363 032	0.672 285 202 673	0.812 529 692 986	0.224 345 992 159
7	0.698 459 489 246	0.713 573 950 794	0.839 330 907 375	0.292 806 902 950
8	0.733 243 927 216	0.745 682 316 102	0.859 432 882 632	0.351 338 353 673
9	?	0.771 356 857 232	0.875 067 710 677	0.401 531 82

Relations (3.1) and (3.2) must also be modified to take into account the 45° rotation; the latter introduces an extra factor of two in the unit of area, so that $f_0(L) = -4\log 2$ and

$$\frac{1}{2^{2L}}\lambda(L) = 1 - \frac{\pi\tilde{x}_2}{L} + o(L^{-1}). \tag{4.1}$$

This factor of two alone increases the accuracy of the measurement of $\tilde{x}_2$ compared to the other two cases, since the corrections are expected to be smaller.

5. Numerical results

We show in table 1 the size of the reduced transfer matrix for $4 \leqslant L \leqslant 9$, in the three cases presented above (sections 4.1–4.3). While the full matrix is very roughly of size 2^{3^L}, the size of the reduced matrix seems to grow as $L!$, which is still large but not as intractable. It is interesting to note that $s_2 < s_1$, that is the modification of the lattice to allow configurations where paths touch at a point *decreases* the number of states.

We have no deep explanation for the remarkable equality of sizes of algorithms 2 and 3, except the observed fact that the states generated are the same in the two cases.

Next we present the data for the largest eigenvalue of the transfer matrix in table 2 with a 12 digit accuracy.

In order to study the asymptotic behaviour of these series of numbers, we use equation (3.2) for cases 1 and 2 (or (4.1) for case 3) to extract approximate values of $\tilde{x}_2$. The results are shown in figure 10. We also presented quadratic fits of these data.

Several remarks are in order. First the two curves corresponding to the square lattice with its regular orientation (with or without contacts at points) seem to converge nicely within the range allowed by the fits. This means that the value of $\tilde{x}_2$ is *not* affected by this modification. However, it is clear that the next corrections to λ_1 and λ_2 are quite different. Second, it is again manifest in figure 10 that the third set of data, corresponding to the 45° rotated square lattice, reaches its limit much faster than the other two. Whereas various fits will give a limiting value for the first two anywhere between 0.355 and 0.36, the range is limited to 0.3563–0.3575 for the latter. Assuming all these limits to be the same, we reach the estimate (1.1) mentioned in

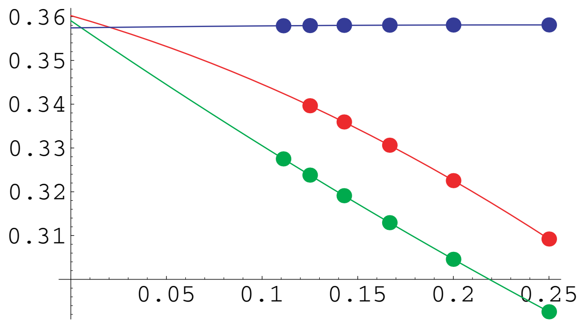

Figure 10. Values of $\tilde{x}_2$ obtained from the eigenvalues of the transfer matrices (table 2) for case 1 (middle curve), case 2 (lower curve) and case 3 (upper curve).

the introduction. Note that there is no simple way for us to evaluate error bars since the results are entirely dependent on the fits used, the latter being arbitrary without any knowledge about the subleading corrections.

Finally, numerical estimates of the norms of higher eigenvalues of the transfer matrix spectra can be extracted by a standard iteration/orthogonalization procedure [26]. Using this method, complex eigenvalues are characterized by an oscillatory behaviour and thus can be discarded (we expect physical observables to be linked to real eigenvalues). Specializing to case 3 (cf section 4.3 above), we find the fourth eigenvalue (in norm) to be the second real one. Its finite-size scaling is well fitted by (2.1), defining a critical index

$$\tilde{x}_2' = 2.35 \pm 0.1. \tag{5.1}$$

This is consistent with the conformal dimension of a level two descendent of the backbone operator.

Extracting the scaling dimensions for even higher eigenvalues becomes increasingly problematic, as the finite-size effects get considerably stronger. It should, however, be noted that the third real eigenvalue is doubly degenerate for any width $L \geqslant 4$. This is supposed to have implications for the organization of the conformal tower of the backbone operator.

Acknowledgments

JLJ is grateful to Jean Vannimenus for interesting discussions during an early stage of this project and wishes to thank Hubert Saleur for drawing his attention to the importance of studying higher eigenvalues. PZ-J would like to thank Claude Jacquemin for introducing him to the mysteries of sockets.

Appendix A. Structure of some small-size transfer matrices

As an illustration of the algorithm explained in this paper, we provide here the simplest non-trivial transfer matrices obtained with the geometries of sections 4.2 and 4.3. They correspond to a strip length $L = 4$ and their size is $s = 12$.

The *basis* in which these matrices are expressed is described in figure 11.

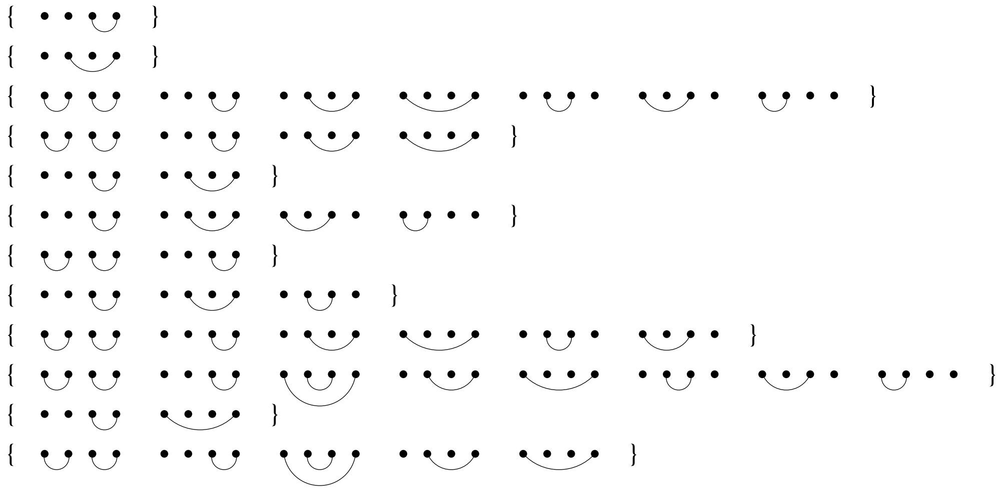

Figure 11. Basis states (up to overall dihedral transformations) for $L = 4$.

The matrices themselves read

$$
\mathbf{T}_2 = \begin{pmatrix}
8 & 0 & 8 & 4 & 4 & 4 & 6 & 8 & 6 & 8 & 8 & 4 \\
0 & 4 & 2 & 1 & 2 & 2 & 0 & 2 & 2 & 2 & 0 & 1 \\
4 & 0 & 8 & 8 & 4 & 9 & 5 & 4 & 5 & 4 & 8 & 6 \\
8 & 0 & 8 & 10 & 6 & 8 & 10 & 8 & 8 & 8 & 12 & 8 \\
8 & 16 & 16 & 12 & 16 & 20 & 6 & 16 & 18 & 16 & 8 & 12 \\
4 & 8 & 8 & 8 & 10 & 18 & 3 & 8 & 11 & 8 & 4 & 8 \\
8 & 0 & 8 & 4 & 4 & 4 & 10 & 8 & 6 & 8 & 8 & 4 \\
8 & 8 & 28 & 13 & 12 & 16 & 6 & 20 & 22 & 28 & 14 & 13 \\
8 & 0 & 24 & 10 & 6 & 8 & 10 & 16 & 20 & 24 & 12 & 8 \\
8 & 20 & 62 & 34 & 26 & 47 & 8 & 34 & 56 & 66 & 18 & 38 \\
0 & 0 & 0 & 1 & 0 & 0 & 0 & 0 & 0 & 0 & 2 & 1 \\
0 & 8 & 4 & 7 & 6 & 8 & 0 & 4 & 6 & 4 & 2 & 9
\end{pmatrix}
$$

$$
\mathbf{T}_3 = \begin{pmatrix}
36 & 24 & 32 & 19 & 28 & 24 & 24 & 40 & 28 & 32 & 33 & 19 \\
9 & 18 & 18 & 12 & 15 & 16 & 7 & 18 & 17 & 18 & 12 & 12 \\
2 & 7 & 8 & 13 & 8 & 14 & 6 & 1 & 2 & 0 & 9 & 7 \\
10 & 12 & 0 & 14 & 13 & 12 & 18 & 6 & 6 & 0 & 12 & 8 \\
36 & 48 & 24 & 38 & 49 & 52 & 30 & 40 & 38 & 24 & 34 & 34 \\
6 & 11 & 2 & 9 & 12 & 18 & 6 & 5 & 6 & 2 & 6 & 9 \\
12 & 8 & 0 & 0 & 6 & 0 & 12 & 8 & 0 & 0 & 7 & 0 \\
10 & 12 & 84 & 39 & 24 & 44 & 12 & 48 & 64 & 84 & 32 & 44 \\
6 & 4 & 32 & 13 & 9 & 12 & 6 & 26 & 30 & 32 & 14 & 11 \\
1 & 0 & 39 & 16 & 6 & 19 & 3 & 16 & 34 & 47 & 5 & 27 \\
0 & 0 & 0 & 7 & 3 & 6 & 4 & 0 & 3 & 0 & 6 & 6 \\
0 & 0 & 0 & 7 & 3 & 6 & 0 & 0 & 3 & 0 & 2 & 10
\end{pmatrix}.
$$

References

[1] Stauffer D and Aharony A 1992 *Introduction to Percolation Theory* (London: Taylor and Francis)
[2] Kasteleyn P W and Fortuin C M 1969 *J. Phys. Soc. Japan* **46** 11
[3] Baxter R J 1982 *Exactly Solved Models in Statistical Mechanics* (London: Academic)
[4] Nienhuis B 1987 *Phase Transitions and Critical Phenomena* vol 11 ed C Domb and J L Lebowitz (London: Academic)
[5] Coniglio A 1982 *J. Phys. A: Math. Gen.* **15** 3829
[6] den Nijs M P M 1979 *J. Phys. A: Math. Gen.* **12** 1857
[7] Nienhuis B, Riedel E K and Schick M 1980 *J. Phys. A: Math. Gen.* **13** L189
[8] Belavin A A, Polyakov A M and Zamolodchikov A B 1984 *Nucl. Phys.* B **241** 333
[9] Saleur H and Duplantier B 1987 *Phys. Rev. Lett.* **58** 2325
[10] Aizenman M, Duplantier B and Aharony A 1999 *Preprint* cond-mat/9901018
[11] Duplantier B and Saleur H 1987 *Nucl. Phys.* B **290** 291
[12] Cardy J L 1992 *J. Phys. A: Math. Gen.* **25** L201
[13] Smirnov S 2001 *C. R. Acad. Sci., Paris* ser 1 *Math.* **333** 239–44
[14] Havlin S and Bunde A 1991 Percolation II *Fractals and Disordered Systems* ed A Bunde and S Havlin (Berlin: Springer)
[15] Grassberger P 1992 *J. Phys. A: Math. Gen.* **25** 5475
[16] Grassberger P 1999 *Physica* A **262** 251 (cond-mat/9808095 v2)
[17] Cardy J L 1983 *J. Phys. A: Math. Gen.* **16** L355
[18] Jacobsen J L and Zinn-Justin P 2002 in preparation
[19] Lawler G F, Schramm O and Werner W 2001 *Preprint* math.PR/0108211
[20] Blöte H W J and Nienhuis B 1989 *J. Phys. A: Math. Gen.* **22** 1415
[21] Blöte H W J and Nightingale M P 1982 *Physica* A **112** 405
[22] Jacobsen J L and Cardy J L 1998 *Nucl. Phys.* B **515** 701
[23] Enting I G 1980 *J. Phys. A: Math. Gen.* **13** 3713
Derrida B 1981 *J. Phys. A: Math. Gen.* **14** L5
[24] Motzkin T 1948 *Bull. Am. Math. Soc.* **54** 352
[25] Dotsenko Vl S, Jacobsen J L, Lewis M-A and Picco M 1999 *Nucl. Phys.* B **546**
Dotsenko Vl S, Jacobsen J L, Lewis M-A and Picco M 1999 *Nucl. Phys.* B **505**
[26] Furstenberg H 1963 *Trans. Am. Math. Soc.* **68** 377
Benettin G, Galgani L, Giorgilli A and Strelcyn J-M 1980 *Meccanica* **15** 9